Elastic response of an acoustic coating on a rib-stiffened plate

Andrew J. Hull *, John R. Welch [1]

Autonomous and Defensive Systems Department, Naval Undersea Warfare Center Division, Newport, RI 02841, USA

ARTICLE INFO

ABSTRACT

This paper develops a three-dimensional analytical model of a fluid-loaded acoustic coating affixed to a rib-stiffened plate. The system is loaded by a plane wave that is harmonic both spatially and temporally. The model begins with Navier–Cauchy equations of motion for an elastic solid, which produces displacement fields that have unknown wave propagation coefficients. These are inserted into stress equations at the boundaries of the plate and the acoustic coating. These stress fields are coupled to the fluid field and the rib stiffeners with force balances. Manipulation of these equations develops an infinite number of indexed equations that are truncated and incorporated into a global matrix equation. This global matrix equation can be solved to determine the wave propagation coefficients. This produces analytical solutions to the systems' displacements, stresses, and scattered pressure field. This model, unlike previously developed analytical models, has elastic behavior and thus incorporates higher order wave motion that makes it accurate at higher wavenumbers and frequencies. An example problem is investigated for three specific model results: (1) the dynamic response, (2) a sonar array embedded in the acoustic coating, and (3) the scattered pressure field. An expression for the high frequency limitation of the model is derived. It is shown that the ribs can have a significant impact on the structural acoustic response of the system.

Published by Elsevier Ltd.

1. Introduction

Underwater vehicle hulls are typically metallic with acoustic coatings that are made of a soft polymer material. These hulls are usually internally reinforced in one direction to provide increased stiffness against the hydrostatic forces that act on the hull when the vessel is submerged. Acoustic coatings are used to produce quieter vehicles, contain sonar sensors, inhibit drag, and prevent biological fouling on the exterior of the vehicle. Understanding the structural response of such a system is important for the design of new underwater vehicles and analysis of existing underwater vehicles. An analytical model with this type of configuration will allow predictions of the dynamic response of an acoustic coating on a marine structure and a sonar system embedded in the coating. Over the years there has been a progression of modeling these systems, from thin unreinforced structures to thick unreinforced structures and thin reinforced structures. The specific problem of an analytical model of a thick reinforced structure has not been previously addressed.

The research of plate theory has been an ongoing field of study for many years. Thin beam (Euler–Bernoulli) theory originates in the eighteenth century [1]. This model is sometimes called a flexural wave model, and an extremely similar model exists in plate theory. Mindlin [2] modified thin plate theory to include the dynamics of rotary inertia and shear

---

* Corresponding author. Tel.: +1 401 832 5189; fax: +1 401 832 2525.
  E-mail addresses: andrew.hull@navy.mil (A.J. Hull), john.r.welch@navy.mil (J.R. Welch).
  [1] Tel.: +401 832 7973; fax: +401 832 2146.

Report Documentation Page

Public reporting burden for the collection of information is estimated to average 1 hour per response, including the time for reviewing instructions, searching existing data sources, gathering and maintaining the data needed, and completing and reviewing the collection of information. Send comments regarding this burden estimate or any other aspect of this collection of information, including suggestions for reducing this burden, to Washington Headquarters Services, Directorate for Information Operations and Reports, 1215 Jefferson Davis Highway, Suite 1204, Arlington VA 22202-4302. Respondents should be aware that notwithstanding any other provision of law, no person shall be subject to a penalty for failing to comply with a collection of information if it does not display a currently valid OMB control number.

1. REPORT DATE **2010**	2. REPORT TYPE	3. DATES COVERED **00-00-2010 to 00-00-2010**

4. TITLE AND SUBTITLE **Elastic Response of an Acoustic Coating on a Rib-Stiffened Plate**	5a. CONTRACT NUMBER
	5b. GRANT NUMBER
	5c. PROGRAM ELEMENT NUMBER
6. AUTHOR(S)	5d. PROJECT NUMBER
	5e. TASK NUMBER
	5f. WORK UNIT NUMBER

7. PERFORMING ORGANIZATION NAME(S) AND ADDRESS(ES) **Autonomous and Defensive Systems Department,Naval Undersea Warfare Center,Newport ,RI,02841**	8. PERFORMING ORGANIZATION REPORT NUMBER

9. SPONSORING/MONITORING AGENCY NAME(S) AND ADDRESS(ES)	10. SPONSOR/MONITOR'S ACRONYM(S)
	11. SPONSOR/MONITOR'S REPORT NUMBER(S)

12. DISTRIBUTION/AVAILABILITY STATEMENT
Approved for public release; distribution unlimited

13. SUPPLEMENTARY NOTES

14. ABSTRACT

15. SUBJECT TERMS

16. SECURITY CLASSIFICATION OF:			17. LIMITATION OF ABSTRACT	18. NUMBER OF PAGES	19a. NAME OF RESPONSIBLE PERSON
a. REPORT **unclassified**	b. ABSTRACT **unclassified**	c. THIS PAGE **unclassified**	**Same as Report (SAR)**	**20**	

effects, and this extended the low frequency and wavenumber region of the model. Analysis of wave propagation in fully elastic plates consisting of one or multiple layers using the Navier–Cauchy equations of motion has been studied extensively and is well documented [3]. Fluid loading has been added to thin plate analysis [4] and thick plate single and multilayer analysis [5]. Using these techniques, the dynamic response of fluid-loaded acoustic coating on an unreinforced plate can be calculated and analyzed for both thin and thick structures.

Over the years, thin plate theory has been expanded to include stiffening effects of ribs that are typical of many marine and aviation structures. These ribs are almost inclusively placed on one side of the plate to reinforce the structure. The response of a periodically supported beam to a load with fixed wavenumber and frequency has been investigated [6]. The response of periodically stiffened fluid-loaded plates to harmonic loading [7] and line and point forces [8] has been established. The problem of aperiodicity in the stiffeners has been solved [9]. This problem was also investigated for a finite number of equally spaced stiffeners [10] and randomly spaced stiffeners [11]. Asymptotic models of plate radiation into fluid fields have also been developed [12]. The problem of an arbitrary number of dissimilar ribs which are randomly spaced has been solved [13]. A model of radiation of sound from a reinforced plate subjected to a line load has been developed [14]. In this paper, the author incorporated the size of the ribs into the analysis of the radiated sound field. Sound radiation from a plate reinforced by infinite sets of orthogonal ribs has been studied [15]. A similar problem with doubly periodic orthogonal ribs has been studied with respect to the diffraction of an incoming plane wave [16]. It is noted that these papers with reinforcing ribs [6–16] use some form of thin plate theory, and the resulting frequency limit where the model assumptions are valid depends on the thickness of the plate, but for most plates it is typically in the hundreds of Hertz. These thin plate theories are based on a single flexural wave traveling in the plate, and do not include the dynamics of higher order wave motion.

The acoustic response of a fully elastic cylindrical shell with a complete acoustic coating has been researched [17] as well as that of a cylindrical shell with a partial acoustic coating [18]. Rib effects are not present in either of these papers. Higher frequency analysis is possible using numerical methods such as finite element analysis [19]; however, these computations can be time consuming and frequently have stability problems when Poisson's ratio of the coating material approaches one half. Recently, a fully elastic solution to a thick plate containing discrete masses was developed [20]. This method can be extended to model the behavior of an acoustic coating on a ribbed backing plate.

This paper derives an analytical model of a reinforced elastic plate system. This model was specifically developed so that this system could undergo analysis at higher wavenumbers and frequencies. Previously, only the low wavenumber and low frequency region of this system was available for analytical modeling. This is of interest because many sonar systems operate at frequencies well above the limits of flexural wave dynamics and if the structure is reinforced, traditional thick plate theory does not include the dynamics of the stiffeners. If the system has fairly rigid stiffeners, then their effects must be incorporated into the model. The work here was developed so that the structural acoustic analysis of underwater vehicles could be accomplished at elastic wavenumbers and frequencies using an analytical model.

The modeled system consists of a plate in contact with a fluid-loaded acoustic coating on one side and a series of equally spaced ribs on the other side. The structure is loaded via the fluid with an incoming acoustic wave. The plate and the acoustic coating are modeled as three-dimensional fully elastic solid bodies, the fluid is modeled as a three-dimensional acoustic field, and the ribs are modeled using the Timoshenko beam equation, the torsional wave equation and the bar wave equation. The formulation begins with elasticity theory where the motion in the plate and the acoustic coating are modeled as a combination of dilatational and shear waves. These waveforms can be used to determine the three-dimensional displacement fields with unknown coefficients. These displacements are inserted into stress and continuity equations at the system boundaries and interfaces that contain the system excitation, the fluid loading, and the force of the ribs on the structure. Using an orthogonalization procedure produces an m-indexed mathematical model of the system where each m index is a set of equations 12 rows by an infinite number of columns. All of the m-indexed equations can be combined and this yields a matrix system of infinite extent, which is truncated to a finite number of terms. Inverting this matrix solves for the unknown coefficients and produces system displacements, stresses, and pressure field solutions. The elastic model is compared to a previously developed thin plate model at low frequency and wavenumbers to insure accuracy and consistency to prior work. A numerical example problem is then studied with specific interest in dynamic response of the structure, reception of acoustic signals and strength of the scattered field. The frequency limitation of the new elastic model is discussed. It is shown that the ribs can significantly affect the system response.

2. Governing equations

The system model is that of a fluid-loaded solid layer, called the acoustic coating, in contact with a rib-stiffened solid layer, called the backing plate, as shown in Fig. 1. This problem is analytically modeled by assuming the pressure in the fluid is governed by the acoustic wave equation, both solid layers are governed by fully elastic equations of motion, and the rib stiffeners are modeled using the Timoshenko beam equation for the bending motion, the torsional wave equation for the twisting motion, and the bar wave equation for the longitudinal motion. The acoustic coating is excited on the top surface with an incoming acoustic wave. The ribs on the bottom of the backing plate are equally spaced at a distance of L in the x-direction. The model uses the following assumptions: (1) the excitation or forcing function acting on the plate is a plane wave at definite wavenumbers in the x- and y-directions and frequency in time, (2) the displacement in both plates is
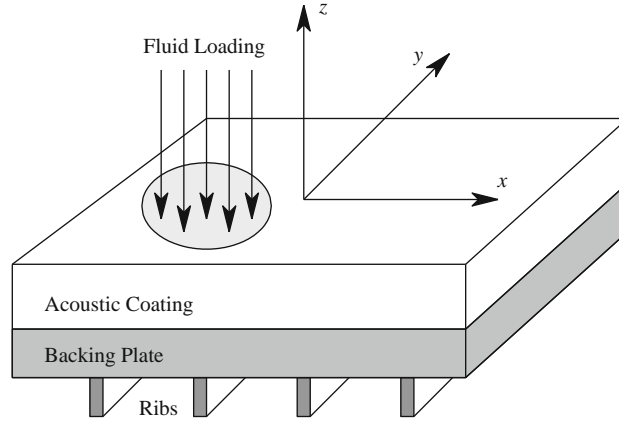
Fig. 1. Schematic of modeled system showing coordinate system.

three-dimensional, (3) both plates have infinite spatial extent in the entire x- and y-directions, (4) the fluid medium has infinite spatial extent in the entire x- and y-directions and infinite spatial extent in the positive z-direction, (5) the interface of the acoustic coating and the backing plate have equivalent displacements and stresses, (6) the motion of the ribs is independent in three directions and is composed of twisting along the y-axis, extension in the y-direction, and bending in the z-direction, and (7) the particle motion is linear, and (8) the fluid medium is lossless.

The motions of both the backing plate and the acoustic coating are governed the Navier–Cauchy equations of motion written in vector form as

$$\mu\nabla^2\mathbf{u}(x,y,z,t)+(\lambda+\mu)\nabla\nabla\cdot\mathbf{u}(x,y,z,t)=\rho\frac{\partial^2\mathbf{u}(x,y,z,t)}{\partial t^2},\tag{1}$$

where ρ is the density, λ and μ are the (usually complex) Lamé constants, t is time, $\cdot$ denotes a vector dot product, and $\mathbf{u}(x,y,z,t)$ is the three-dimensional Cartesian coordinate displacement vector. Using standard techniques [21] to solve Eq. (1) and incorporating the periodicity of the system [6] into the solution yields the displacements as

$$u_j(x,y,z,t)=\sum_{m=-\infty}^{m=+\infty}U_m^{(j)}(z)\exp(\mathrm{i}k_m x)\exp(\mathrm{i}k_y y)\exp(-\mathrm{i}\omega t),\tag{2}$$

$$v_j(x,y,z,t)=\sum_{m=-\infty}^{m=+\infty}V_m^{(j)}(z)\exp(\mathrm{i}k_m x)\exp(\mathrm{i}k_y y)\exp(-\mathrm{i}\omega t),\tag{3}$$

and

$$w_j(x,y,z,t)=\sum_{m=-\infty}^{m=+\infty}W_m^{(j)}(z)\exp(\mathrm{i}k_m x)\exp(\mathrm{i}k_y y)\exp(-\mathrm{i}\omega t),\tag{4}$$

where

$$k_m=k_x+\frac{2\pi m}{L},\tag{5}$$

where k_x is wavenumber with respect to the x-axis, k_y is the wavenumber with respect to the y-axis, ω is frequency, t is time, $\mathrm{i}=\sqrt{-1}$ and j is either 1, which corresponds to the backing plate or 2, which corresponds to the acoustic coating. The functions $U_m^{(j)}(z)$, $V_m^{(j)}(z)$, and $W_m^{(j)}(z)$ are given by

$$U_m^{(j)}(z)=A_m^{(j)}\mathrm{i}k_m\cos[\alpha_m^{(j)}z]+B_m^{(j)}\mathrm{i}k_m\sin[\alpha_m^{(j)}z]+C_m^{(j)}\frac{k_m k_y}{\beta_m^{(j)}}\sin[\beta_m^{(j)}z]-D_m^{(j)}\frac{k_m k_y}{\beta_m^{(j)}}\cos[\beta_m^{(j)}z]$$
$$+E_m^{(j)}\left[\beta_m^{(j)}+\frac{k_y^2}{\beta_m^{(j)}}\right]\sin[\beta_m^{(j)}z]-F_m^{(j)}\left[\beta_m^{(j)}+\frac{k_y^2}{\beta_m^{(j)}}\right]\cos[\beta_m^{(j)}z],\tag{6}$$

$$V_m^{(j)}(z)=A_m^{(j)}\mathrm{i}k_y\cos[\alpha_m^{(j)}z]+B_m^{(j)}\mathrm{i}k_y\sin[\alpha_m^{(j)}z]-C_m^{(j)}\left[\beta_m^{(j)}+\frac{k_m^2}{\beta_m^{(j)}}\right]\sin[\beta_m^{(j)}z]+D_m^{(j)}\left[\beta_m^{(j)}+\frac{k_m^2}{\beta_m^{(j)}}\right]\cos[\beta_m^{(j)}z]$$
$$-E_m^{(j)}\frac{k_m k_y}{\beta_m^{(j)}}\sin[\beta_m^{(j)}z]+F_m^{(j)}\frac{k_m k_y}{\beta_m^{(j)}}\cos[\beta_m^{(j)}z]\tag{7}$$

and

$$W_m^{(j)}(z) = -A_m^{(j)}\alpha_m^{(j)}\sin[\alpha_m^{(j)}z] + B_m^{(j)}\alpha_m^{(j)}\cos[\alpha_m^{(j)}z] - C_m^{(j)}\mathrm{i}k_y\cos[\beta_m^{(j)}z] - D_m^{(j)}\mathrm{i}k_y\sin[\beta_m^{(j)}z]$$
$$+ E_m^{(j)}\mathrm{i}k_m\cos[\beta_m^{(j)}z] + F_m^{(j)}\mathrm{i}k_m\sin[\beta_m^{(j)}z], \tag{8}$$

where $\alpha_m^{(j)}$ is the modified wavenumber associated with the dilatational wave and is expressed as

$$\alpha_m^{(j)} = \sqrt{[k_d^{(j)}]^2 - k_m^2 - k_y^2}, \tag{9}$$

where $k_d^{(j)}$ is the dilatational wavenumber on the layer (j) and is equal to $\omega/c_d^{(j)}$, where $c_d^{(j)}$ is the dilatational wave speed on the layer (j); $\beta_m^{(j)}$ is the modified wavenumber associated with the shear wave and is expressed as

$$\beta_m^{(j)} = \sqrt{[k_s^{(j)}]^2 - k_m^2 - k_y^2}, \tag{10}$$

where $k_s^{(j)}$ is the shear wavenumber on the layer (j) and is equal to $\omega/c_s^{(j)}$, where $c_s^{(j)}$ is the shear wave speed on the layer (j). The dilatational wave speed is given by

$$c_d = \sqrt{\frac{\lambda + 2\mu}{\rho}} \tag{12}$$

and the shear wave speed is determined by

$$c_s = \sqrt{\frac{\mu}{\rho}}. \tag{13}$$

If the model of the layers of the structure contain a structural loss factor, then the dilatational and shear wave speed are complex quantities as are the modified wavenumbers α and β. (Structural loss factors are typically used to model acoustic coatings and sometimes used to model metallic hull behavior.) Note that the positive value of radical is chosen in Eqs. (9) and (10). Choosing the negative value would result in the identical solution because the solid layers are finite in the z-direction. In Eqs. (6)–(8), $A_m^{(j)}$, $B_m^{(j)}$, $C_m^{(j)}$, $D_m^{(j)}$, $E_m^{(j)}$, and $F_m^{(j)}$ are the unknown complex wave propagation coefficients whose solutions we seek.

The acoustic pressure in the fluid medium is governed by the three-dimensional wave equation and is written in Cartesian coordinates as

$$\frac{\partial^2 p_a(x,y,z,t)}{\partial x^2} + \frac{\partial^2 p_a(x,y,z,t)}{\partial y^2} + \frac{\partial^2 p_a(x,y,z,t)}{\partial z^2} - \frac{1}{c_f^2}\frac{\partial^2 p_a(x,y,z,t)}{\partial t^2} = 0, \tag{14}$$

where $p_a(x,y,z,t)$ is the pressure and c_f is the real-valued compressional wave speed in the fluid. The pressure field in the fluid consists of an incoming incident pressure wave (system excitation) applied to the structure at the top ($z=c$) and an outgoing scattered wave that propagates in the positive z-direction. Due to the periodicity of the system, the outgoing pressure wave has the same spatial form as the displacement fields, thus the solution to Eq. (14) is written as

$$p_a(x,y,z,t) = P_I \exp(-\mathrm{i}\gamma_0 z)\exp(\mathrm{i}k_x x)\exp(\mathrm{i}k_y y)\exp(-\mathrm{i}\omega t)$$
$$+ \sum_{m=-\infty}^{m=+\infty} R_m \exp(\mathrm{i}\gamma_m z)\exp(\mathrm{i}k_m x)\exp(\mathrm{i}k_y y)\exp(-\mathrm{i}\omega t), \tag{15}$$

where P_I is the magnitude of the applied pressure field, R_m are unknown wave propagation coefficients, and γ_m is the modified wavenumber associated with the compressional wave in the fluid and is given by

$$\gamma_m = \sqrt{(\omega/c_f)^2 - k_m^2 - k_y^2} = \sqrt{k_f^2 - k_m^2 - k_y^2}. \tag{16}$$

The expression given by Eq. (16) is either purely real or purely imaginary. The positive root of Eq. (16) is associated with the outgoing radiated compressional wave, and when this term is purely imaginary, the sign of the argument of the series terms in Eq. (15) is negative, and this corresponds to a spatially decaying wave in the positive z-direction. The relationship between arrival angles on the plate of an acoustic wave and the x- and y-wavenumbers is determined by

$$k_x = (\omega/c_f)\sin(\theta) = k_f\sin(\theta) \tag{17}$$

and

$$k_y = \sqrt{k_f^2 - k_x^2}\sin(\phi), \tag{18}$$

where θ is the arrival angle of the acoustic wave with respect to the x-axis and ϕ is the arrival angle with respect to the y-axis. Note that the expression under the radical in Eq. (18) is always positive, and that the positive root is used for the analysis. The value of Eq. (18), however, can be negative based on the sign of ϕ. A value of $\theta=\phi=0$ corresponds to a broadside or boresight wave exciting the system.

The displacement of any individual rib in the z-direction is modeled using the Timoshenko beam equation, which is

$$EI\frac{\partial^4 s_z(x,y,t)}{\partial y^4}-\left(\rho I+\frac{\rho IE}{G\kappa}\right)\frac{\partial^4 s_z(x,y,t)}{\partial y^2 \partial t^2}+A\rho\frac{\partial^2 s_z(x,y,t)}{\partial t^2}+\frac{\rho^2 I}{G\kappa}\frac{\partial^4 s_z(x,y,t)}{\partial t^4}=-f_z(x,y,t)+\frac{EI}{GA\kappa}\frac{\partial^2 f_z(x,y,t)}{\partial y^2}-\frac{\rho I}{GA\kappa}\frac{\partial^2 f_z(x,y,t)}{\partial t^2},$$

(19)

where $s_z(x,y,t)$ is the rib displacement in the z-direction, $f_z(x,y,t)$ is the force per unit length in the z-direction, E is Young's modulus, I is the second moment of area about the x-axis, ρ is the density, G is the shear modulus, A is the area, and κ is the shear coefficient. Noting that the rib displacement in the z-direction is equal to the plate displacement at $z=a$ in the z-direction, i.e.

$$s_z(x,y,t)=\sum_{m=-\infty}^{m=+\infty}W_m^{(1)}(a)\exp(ik_m x)\exp(ik_y y)\exp(-i\omega t),$$

(20)

yields the solution to the z-directional force in Eq. (19) as

$$f_z(x,y,t)=K_z\sum_{m=-\infty}^{m=+\infty}W_m^{(1)}(a)\exp(ik_m x)\exp(ik_y y)\exp(-i\omega t)$$

(21)

with

$$K_z=\frac{EIk_y^4-(\rho I+(\rho IE/G\kappa))\omega^2 k_y^2-A\rho\omega^2+(\rho^2 I/G\kappa)\omega^4}{-1-(EI/GA\kappa)k_y^2+(\rho I/GA\kappa)\omega^2},$$

(22)

where K_z has units of stiffness per unit length. Note that the case when the denominator of Eq. (22) equals zero corresponds to the maximum frequency that the Timoshenko beam equation is considered valid. This frequency limitation is discussed in more detail in Section 5.

The rotation of any individual rib is modeled using the torsional wave equation, written with the independent variable as the angle of the rib as

$$\rho J\frac{\partial^2 \theta(x,y,t)}{\partial t^2}-GJ\frac{\partial^2 \theta(x,y,t)}{\partial y^2}=-m_y(x,y,t),$$

(23)

where $\theta(x,y,t)$ is the clockwise angle of rotation of the rib about its centroid, $m_y(x,y,t)$ is the torque per unit length in the y-direction at the top of the rib, and J is the polar moment of inertia about the y-axis. Rewriting the torque expression as

$$m_y(x,y,t)=\left(\frac{h}{2}\right)f_x(x,y,t),$$

(24)

where h is the height of the rib and $f_x(x,y,t)$ is the force per unit length in the x-direction, and assuming that the rib is always at a right angle to the bottom of the backing plate, gives the relationship

$$\theta(x,y,t)=\frac{\partial w_1(x,y,a,t)}{\partial x}=\sum_{m=-\infty}^{m=+\infty}ik_m W_m^{(1)}(a)\exp(ik_m x)\exp(ik_y y)\exp(-i\omega t)$$

(25)

which yields

$$f_x(x,y,t)=\hat{K}_x\sum_{m=-\infty}^{m=+\infty}ik_m W_m^{(1)}(a)\exp(ik_m x)\exp(ik_y y)\exp(-i\omega t)$$

(26)

with

$$\hat{K}_x=\frac{2J}{h}[\omega^2\rho-k_y^2 G],$$

(27)

where $\hat{K}_x$ has units of stiffness and the caret has been added to this constant because it has different units than the stiffness constant in the z-direction.

The displacement of any individual rib in the y-direction is modeled using the longitudinal wave equation of a bar, written as

$$A\rho\frac{\partial^2 s_y(x,y,t)}{\partial t^2}-AE\frac{\partial^2 s_y(x,y,t)}{\partial y^2}=-f_y(x,y,t),$$

(28)

where $s_y(x,y,z)$ is the rib displacement in the y-direction and $f_y(x,y,t)$ is the force per unit length in the y-direction. The rib displacement in the y-direction is equal to the plate displacement at $z=a$ in the y-direction, thus

$$s_y(x,y,t)=\sum_{m=-\infty}^{m=+\infty}V_m^{(1)}(a)\exp(ik_m x)\exp(ik_y y)\exp(-i\omega t)$$

(29)

and this yields the solution to the y-directional force in Eq. (28) as

$$f_y(x,y,t) = K_y \sum_{m=-\infty}^{m=+\infty} V_m^{(1)}(a) \exp(\mathrm{i}k_m x) \exp(\mathrm{i}k_y y) \exp(-\mathrm{i}\omega t) \tag{30}$$

with

$$K_y = A\rho\omega^2 - AEk_y^2, \tag{31}$$

where K_y has units of stiffness per length. Note that the dynamic beam stiffness expressions $\hat{K}_x$, K_y, and K_z can change signs based on the parameters of the beam and that they can be complex quantities if the material properties of the beam are complex. This typically results when a structural damping model is used which produces a complex Young and shear modulus of the beam. For the remainder of the paper, the exponential function with respect to time is suppressed in all the equations.

The solutions to the wave propagation coefficients are determined by formulating the problem using 13 boundary value equations written in terms of the plates' displacements and corresponding forcing functions. The system is loaded on the bottom by the ribs; thus, the normal stress and the shear stresses at this location ($z=a$) are written using a force balance between the forces in the ribs and the bottom of the lower plate. Because there are an infinite number of ribs and they each act as a point force, a Dirac comb function is used to distribute the forces of the ribs discretely in the x-direction. The normal stress is written as

$$\tau_{zz}(x,y,a,t) = \lambda_1 \left[\frac{\partial u_1(x,y,a,t)}{\partial x} + \frac{\partial v_1(x,y,a,t)}{\partial y} + \frac{\partial w_1(x,y,a,t)}{\partial z} \right] + 2\mu_1 \frac{\partial w_1(x,y,a,t)}{\partial z}$$
$$= \sum_{n=-\infty}^{n=+\infty} f_z(x,y,t)\delta(x-nL) \tag{32}$$

and the tangential stresses are written as

$$\tau_{zy}(x,y,a,t) = \mu_1 \left[\frac{\partial v_1(x,y,a,t)}{\partial z} + \frac{\partial w_1(x,y,a,t)}{\partial y} \right] = \sum_{n=-\infty}^{n=+\infty} f_y(x,y,t)\delta(x-nL) \tag{33}$$

and

$$\tau_{zx}(x,y,a,t) = \mu_1 \left[\frac{\partial w_1(x,y,a,t)}{\partial x} + \frac{\partial u_1(x,y,a,t)}{\partial z} \right] = \sum_{n=-\infty}^{n=+\infty} f_x(x,y,t)\delta(x-nL), \tag{34}$$

where $\delta(x-nL)$ is the spatial Dirac delta function, and the subscript 1 corresponds to the backing plate.

The interface between the backing plate and the acoustic coating is modeled using continuity of displacements and stresses. Continuity of the stress fields at the interface ($z=b$) yields

$$\lambda_1 \left[\frac{\partial u_1(x,y,b,t)}{\partial x} + \frac{\partial v_1(x,y,b,t)}{\partial y} + \frac{\partial w_1(x,y,b,t)}{\partial z} \right] + 2\mu_1 \frac{\partial w_1(x,y,b,t)}{\partial z}$$
$$= \lambda_2 \left[\frac{\partial u_2(x,y,b,t)}{\partial x} + \frac{\partial v_2(x,y,b,t)}{\partial y} + \frac{\partial w_2(x,y,b,t)}{\partial z} \right] + 2\mu_2 \frac{\partial w_2(x,y,b,t)}{\partial z}, \tag{35}$$

$$\mu_1 \left[\frac{\partial v_1(x,y,b,t)}{\partial z} + \frac{\partial w_1(x,y,b,t)}{\partial y} \right] = \mu_2 \left[\frac{\partial v_2(x,y,b,t)}{\partial z} + \frac{\partial w_2(x,y,b,t)}{\partial y} \right] \tag{36}$$

and

$$\mu_1 \left[\frac{\partial w_1(x,y,b,t)}{\partial x} + \frac{\partial u_1(x,y,b,t)}{\partial z} \right] = \mu_2 \left[\frac{\partial w_2(x,y,b,t)}{\partial x} + \frac{\partial u_2(x,y,b,t)}{\partial z} \right], \tag{37}$$

where the subscript 2 corresponds to the acoustic coating. Continuity of the displacement fields at the interface yields

$$u_1(x,y,b,t) = u_2(x,y,b,t), \tag{38}$$

$$v_1(x,y,b,t) = v_2(x,y,b,t) \tag{39}$$

and

$$w_1(x,y,b,t) = w_2(x,y,b,t). \tag{40}$$

The top of the acoustic coating is in contact with the fluid, and the normal stress at this location ($z=c$) is written using a force balance between the pressure in the fluid and the coating as

$$\tau_{zz}(x,y,c,t) = \lambda_2 \left[\frac{\partial u_2(x,y,c,t)}{\partial x} + \frac{\partial v_2(x,y,c,t)}{\partial y} + \frac{\partial w_2(x,y,c,t)}{\partial z} \right] + 2\mu_2 \frac{\partial w_2(x,y,c,t)}{\partial z}$$
$$= -p_a(x,y,c,t), \tag{41}$$

where $p_a(x,y,c,t)$ is the pressure field in contact with the top of the plate. Furthermore, this interface satisfies the linear momentum equation, which relates the normal acceleration of the plate surface to the spatial gradient of the pressure field by

$$\rho_f \frac{\partial^2 w_2(x,y,c,t)}{\partial t^2} = -\frac{\partial p_a(x,y,c,t)}{\partial z},$$ (42)

where ρ_f is the density of the fluid. The tangential stresses on the top of the acoustic coating are modeled as free boundary conditions and are written as

$$\tau_{zy}(x,y,c,t) = \mu_2 \left[\frac{\partial v_2(x,y,c,t)}{\partial z} + \frac{\partial w_2(x,y,c,t)}{\partial y} \right] = 0$$ (43)

and

$$\tau_{zx}(x,y,c,t) = \mu_2 \left[\frac{\partial w_2(x,y,c,t)}{\partial x} + \frac{\partial u_2(x,y,c,t)}{\partial z} \right] = 0.$$ (44)

3. Analytical solution

The functional form of the displacement fields in Eqs. (6)–(8) are now inserted into the boundary value equations given by Eqs. (32)–(41) and (43)–(44). Additionally, the pressure field in Eq. (15) and the interface equation listed as Eq. (42) are utilized, and which directly results in the following equations:

$$\lambda_1 \sum_{m=-\infty}^{m=+\infty} ik_m U_m^{(1)}(a) \exp(ik_m x) + \lambda_1 ik_y \sum_{m=-\infty}^{m=+\infty} V_m^{(1)}(a) \exp(ik_m x)$$
$$+ (\lambda_1 + 2\mu_1) \sum_{m=-\infty}^{m=+\infty} \frac{dW_m^{(1)}(a)}{dz} \exp(ik_m x) = K_z \sum_{n=-\infty}^{n=+\infty} [\sum_{m=-\infty}^{m=+\infty} W_m^{(1)}(a) \exp(ik_m x)] \delta(x-nL),$$ (45)

$$\mu_1 \sum_{m=-\infty}^{m=+\infty} \frac{dV_m^{(1)}(a)}{dz} \exp(ik_m x) + \mu_1 ik_y \sum_{m=-\infty}^{m=+\infty} W_m^{(1)}(a) \exp(ik_m x) = K_y \sum_{n=-\infty}^{n=+\infty} [\sum_{m=-\infty}^{m=+\infty} V_m^{(1)}(a) \exp(ik_m x)] \delta(x-nL),$$ (46)

$$\mu_1 \sum_{m=-\infty}^{m=+\infty} ik_m W_m^{(1)}(a) \exp(ik_m x) + \mu_1 \sum_{m=-\infty}^{m=+\infty} \frac{dU_m^{(1)}(a)}{dz} \exp(ik_m x) = \hat{K}_x \sum_{n=-\infty}^{n=+\infty} [\sum_{m=-\infty}^{m=+\infty} ik_m W_m^{(1)}(a) \exp(ik_m x)] \delta(x-nL),$$ (47)

$$\lambda_1 \sum_{m=-\infty}^{m=+\infty} ik_m U_m^{(1)}(b) \exp(ik_m x) + \lambda_1 ik_y \sum_{m=-\infty}^{m=+\infty} V_m^{(1)}(b) \exp(ik_m x) + (\lambda_1 + 2\mu_1) \sum_{m=-\infty}^{m=+\infty} \frac{dW_m^{(1)}(b)}{dz} \exp(ik_m x)$$
$$= \lambda_2 \sum_{m=-\infty}^{m=+\infty} ik_m U_m^{(2)}(b) \exp(ik_m x) + \lambda_2 ik_y \sum_{m=-\infty}^{m=+\infty} V_m^{(2)}(b) \exp(ik_m x) + (\lambda_2 + 2\mu_2) \sum_{m=-\infty}^{m=+\infty} \frac{dW_m^{(2)}(b)}{dz} \exp(ik_m x),$$ (48)

$$\mu_1 \sum_{m=-\infty}^{m=+\infty} \frac{dV_m^{(1)}(b)}{dz} \exp(ik_m x) + \mu_1 ik_y \sum_{m=-\infty}^{m=+\infty} W_m^{(1)}(b) \exp(ik_m x)$$
$$= \mu_2 \sum_{m=-\infty}^{m=+\infty} \frac{dV_m^{(2)}(b)}{dz} \exp(ik_m x) + \mu_2 ik_y \sum_{m=-\infty}^{m=+\infty} W_m^{(2)}(b) \exp(ik_m x),$$ (49)

$$\mu_1 \sum_{m=-\infty}^{m=+\infty} ik_m W_m^{(1)}(b) \exp(ik_m x) + \mu_1 \sum_{m=-\infty}^{m=+\infty} \frac{dU_m^{(1)}(b)}{dz} \exp(ik_m x)$$
$$= \mu_2 \sum_{m=-\infty}^{m=+\infty} ik_m W_m^{(2)}(b) \exp(ik_m x) + \mu_2 \sum_{m=-\infty}^{m=+\infty} \frac{dU_m^{(2)}(b)}{dz} \exp(ik_m x),$$ (50)

$$\sum_{m=-\infty}^{m=+\infty} U_m^{(1)}(b) \exp(ik_m x) = \sum_{m=-\infty}^{m=+\infty} U_m^{(2)}(b) \exp(ik_m x),$$ (51)

$$\sum_{m=-\infty}^{m=+\infty} V_m^{(1)}(b) \exp(ik_m x) = \sum_{m=-\infty}^{m=+\infty} V_m^{(2)}(b) \exp(ik_m x),$$ (52)

$$\sum_{m=-\infty}^{m=+\infty} W_m^{(1)}(b) \exp(ik_m x) = \sum_{m=-\infty}^{m=+\infty} W_m^{(2)}(b) \exp(ik_m x),$$ (53)

$$\lambda_2 \sum_{m=-\infty}^{m=+\infty} ik_m U_m^{(2)}(c)\exp(ik_m x) + \lambda_2 ik_y \sum_{m=-\infty}^{m=+\infty} V_m^{(2)}(c)\exp(ik_m x) + (\lambda_2+2\mu_2) \sum_{m=-\infty}^{m=+\infty} \frac{dW_m^{(2)}(c)}{dz}\exp(ik_m x)$$
$$+ \sum_{m=-\infty}^{m=+\infty} \left(\frac{\omega^2 \rho_f}{i\gamma_m}\right) W_m^{(2)}(c)\exp(ik_m x) = -2P_I \exp(ik_x x), \tag{54}$$

$$\mu_2 \sum_{m=-\infty}^{m=+\infty} \frac{dV_m^{(2)}(c)}{dz}\exp(ik_m x) + \mu_2 ik_y \sum_{m=-\infty}^{m=+\infty} W_m^{(2)}(c)\exp(ik_m x) = 0, \tag{55}$$

and

$$\mu_2 \sum_{m=-\infty}^{m=+\infty} ik_m W_m^{(2)}(c)\exp(ik_m x) + \mu_2 \sum_{m=-\infty}^{m=+\infty} \frac{dU_m^{(2)}(c)}{dz}\exp(ik_m x) = 0. \tag{56}$$

To eliminate the Dirac delta function present in Eqs. (45)–(47), the Fourier series of the Dirac comb function is written as

$$\sum_{n=-\infty}^{n=+\infty} \delta(x-nL) = \frac{1}{L}\sum_{n=-\infty}^{n=+\infty} \exp\left(\frac{i2\pi nx}{L}\right). \tag{57}$$

Furthermore, the identities

$$\sum_{n=-\infty}^{n=+\infty}\left[\sum_{m=-\infty}^{m=+\infty}\left\{\begin{array}{c} W_m^{(1)}(a) \\ V_m^{(1)}(a) \\ ik_m W_m^{(1)}(a) \end{array}\right\}\exp(ik_m x)\right]\exp\left(\frac{i2\pi nx}{L}\right) = \left[\sum_{n=-\infty}^{n=+\infty}\left\{\begin{array}{c} W_n^{(1)}(a) \\ V_n^{(1)}(a) \\ ik_n W_n^{(1)}(a) \end{array}\right\}\right]\sum_{m=-\infty}^{m=+\infty}\exp(ik_m x) \tag{58}$$

are also applied to Eqs. (45)–(47) to separate the embedded double summation into two multiplicative summations. A proof of Eq. (58) is given in Appendix A. This modified version of Eqs. (45)–(47), with Eqs. (48)–(56) are all multiplied by $\exp(-ik_p x)$ and integrated over $[0,L]$. Because the exponential functions are orthogonal on this interval, the equations decouple into sets of m-indexed equations, each one expressed as

$$\lambda_1 ik_m U_m^{(1)}(a) + \lambda_1 ik_y V_m^{(1)}(a) + (\lambda_1+2\mu_1)\frac{dW_m^{(1)}(a)}{dz} = \frac{K_z}{L}\sum_{n=-\infty}^{n=+\infty} W_n^{(1)}(a), \tag{59}$$

$$\mu_1 \frac{dV_m^{(1)}(a)}{dz} + \mu_1 ik_y W_m^{(1)}(a) = \frac{K_y}{L}\sum_{n=-\infty}^{n=+\infty} V_n^{(1)}(a), \tag{60}$$

$$\mu_1 ik_m W_m^{(1)}(a) + \mu_1 \frac{dU_m^{(1)}(a)}{dz} = \frac{\hat{K}_x}{L}\sum_{n=-\infty}^{n=+\infty} ik_n W_n^{(1)}(a), \tag{61}$$

$$\lambda_1 ik_m U_m^{(1)}(b) + \lambda_1 ik_y V_m^{(1)}(b) + (\lambda_1+2\mu_1)\frac{dW_m^{(1)}(b)}{dz} - \lambda_2 ik_m U_m^{(2)}(b) - \lambda_2 ik_y V_m^{(2)}(b) - (\lambda_2+2\mu_2)\frac{dW_m^{(2)}(b)}{dz} = 0, \tag{62}$$

$$\mu_1 \frac{dV_m^{(1)}(b)}{dz} + \mu_1 ik_y W_m^{(1)}(b) - \mu_2 \frac{dV_m^{(2)}(b)}{dz} - \mu_2 ik_y W_m^{(2)}(b) = 0, \tag{63}$$

$$\mu_1 ik_m W_m^{(1)}(b) + \mu_1 \frac{dU_m^{(1)}(b)}{dz} - \mu_2 ik_m W_m^{(2)}(b) - \mu_2 \frac{dU_m^{(2)}(b)}{dz} = 0, \tag{64}$$

$$U_m^{(1)}(b) - U_m^{(2)}(b) = 0, \tag{65}$$

$$V_m^{(1)}(b) - V_m^{(2)}(b) = 0, \tag{66}$$

$$W_m^{(1)}(b) - W_m^{(2)}(b) = 0, \tag{67}$$

$$\lambda_2 ik_m U_m^{(2)}(c) + \lambda_2 ik_y V_m^{(2)}(c) + (\lambda_2+2\mu_2)\frac{dW_m^{(2)}(c)}{dz} + \left(\frac{\omega^2 \rho_f}{i\gamma_m}\right)W_m^{(2)}(c) = \begin{cases} -2P_I, & m=0, \\ 0, & m\neq 0. \end{cases} \tag{68}$$

$$\mu_2 \frac{dV_m^{(2)}(c)}{dz} + \mu_2 ik_y W_m^{(2)}(c) = 0, \tag{69}$$

and

$$\mu_2 ik_m W_m^{(2)}(c) + \mu_2 \frac{dU_m^{(2)}(c)}{dz} = 0. \tag{70}$$

Note that the left-hand side of Eqs. (59)–(70) are m indexed and the right-hand side of Eqs. (59)–(61) are n summed. Physically, the left-hand side of these equations model the acoustic coating and backing plate, the right-hand side of Eqs. (59)–(61) models the ribs, and the right-hand side of Eq. (68) models the incoming acoustic energy.

The functional forms of the displacements given in Eqs. (6)–(8) are inserted into Eqs. (59)–(70) and the resulting algebraic matrix equation for each set of m-indexed coefficients is

$$[\mathbf{A}(k_m)]\{\mathbf{x}_m\} = \sum_{n=-\infty}^{n=+\infty} [\mathbf{F}(k_n)]\{\mathbf{x}_n\} + \begin{cases} \{\mathbf{p}\}, & m = 0, \\ \mathbf{0}, & m \neq 0, \end{cases} \tag{71}$$

where $[\mathbf{A}(k_m)]$ is a 12×12 matrix that models the dynamics of the backing plate and the acoustic coating, $\{\mathbf{x}_m\}$ is the 12×1 vector of unknown wave propagation coefficients, $[\mathbf{F}(k_n)]$ is the 12×12 matrix that models the dynamic interaction of the ribs and the backing plate, and $\{\mathbf{p}\}$ is the 12×1 vector that models the incoming acoustic wave acting on the structure. The entries of the matrices and vectors in Eq. (71) are listed in Appendix B. Eq. (71) is now written for all values of the index m and the results are rewritten in global matrix form. This mathematical process is previously described [20] and this results in

$$\hat{\mathbf{A}}\hat{\mathbf{x}} = \hat{\mathbf{F}}\hat{\mathbf{x}} + \hat{\mathbf{p}}, \tag{72}$$

where $\hat{\mathbf{A}}$ is a block diagonal matrix and is written as

$$\hat{\mathbf{A}} = \begin{bmatrix} \ddots & & \vdots & & \iddots \\ & \mathbf{A}(k_{-1}) & \mathbf{0} & \mathbf{0} & \\ \cdots & \mathbf{0} & \mathbf{A}(k_0) & \mathbf{0} & \cdots \\ & \mathbf{0} & \mathbf{0} & \mathbf{A}(k_1) & \\ \iddots & & \vdots & & \ddots \end{bmatrix}. \tag{73}$$

$\hat{\mathbf{F}}$ is a rank deficient, block partitioned matrix and is equal to

$$\hat{\mathbf{F}} = \begin{bmatrix} \ddots & & \vdots & & \iddots \\ & \mathbf{F}(k_{-1}) & \mathbf{F}(k_0) & \mathbf{F}(k_1) & \\ \cdots & \mathbf{F}(k_{-1}) & \mathbf{F}(k_0) & \mathbf{F}(k_1) & \cdots \\ & \mathbf{F}(k_{-1}) & \mathbf{F}(k_0) & \mathbf{F}(k_1) & \\ \iddots & & \vdots & & \ddots \end{bmatrix}. \tag{74}$$

$\hat{\mathbf{p}}$ is the system excitation vector and is written as

$$\hat{\mathbf{p}} = [\cdots \quad \mathbf{0}^{\mathrm{T}} \quad \mathbf{p}^{\mathrm{T}} \quad \mathbf{0}^{\mathrm{T}} \quad \cdots]^{\mathrm{T}} \tag{75}$$

and $\hat{\mathbf{x}}$ is the vector that contains the unknown wave propagation coefficients and is equal to

$$\hat{\mathbf{x}} = [\cdots \quad \{\mathbf{x}_{-1}\}^{\mathrm{T}} \quad \{\mathbf{x}_0\}^{\mathrm{T}} \quad \{\mathbf{x}_1\}^{\mathrm{T}} \quad \cdots]^{\mathrm{T}}, \tag{76}$$

where

$$\{\mathbf{x}_0\} = \left\{ A_0^{(1)} \quad B_0^{(1)} \quad C_0^{(1)} \quad D_0^{(1)} \quad E_0^{(1)} \quad F_0^{(1)} \quad A_0^{(2)} \quad B_0^{(2)} \quad C_0^{(2)} \quad D_0^{(2)} \quad E_0^{(2)} \quad F_0^{(2)} \right\}^{\mathrm{T}}. \tag{77}$$

The $\mathbf{0}$ term in Eq. (73) is a 12×12 matrix with all zero entries and the $\mathbf{0}$ term in Eq. (75) is a 12×1 vector with all zero entries. The solution to the wave propagation coefficients is now found by truncating the matrices in Eq. (72) to a finite number of terms and solving

$$\hat{\mathbf{x}} = [\hat{\mathbf{A}} - \hat{\mathbf{F}}]^{-1}\hat{\mathbf{p}}. \tag{78}$$

Once these are known, the displacement field of the system in the spatial domain can be determined using Eqs. (2)–(8). Furthermore, the stress distribution in the backing plate, acoustic coating and the scattered acoustic field can be computed.

4. Model validation

The elastic model that has been developed in Sections 2 and 3 can be compared to a fluid-loaded, ribbed, Bernoulli–Euler thin plate model that has been previously developed [7–9]. This will provide validation of the model for low frequencies, low wavenumbers, and small plate thicknesses. This Bernoulli–Euler model, however, only incorporates flexural wave behavior, making the model assumptions invalid at higher frequencies and wavenumbers. The thin plate model has one degree-of-freedom that is displacement in the z-direction and is a constant value across the thickness of the plate. This displacement equation is written as

$$w(x,y) = \sum_{m=-\infty}^{m=+\infty} W_m \exp(\mathrm{i}k_m x) \exp(\mathrm{i}k_y y) \tag{79}$$

and this displacement field can be determined by

$$\{\mathbf{w}\} = [\mathbf{T} + \mathbf{K} + \mathbf{R}]^{-1}\{\mathbf{f}\}, \tag{80}$$

where

$$\{\mathbf{w}\} = \left\{ \cdots \quad W_{-1} \quad W_0 \quad W_1 \quad \cdots \right\}^T, \tag{81}$$

$$[\mathbf{T}] = \begin{bmatrix} \ddots & & \vdots & & \iddots \\ & T_{-1} & 0 & 0 & \\ \cdots & 0 & T_0 & 0 & \cdots \\ & 0 & 0 & T_1 & \\ \iddots & & \vdots & & \ddots \end{bmatrix}, \tag{82}$$

$$[\mathbf{K}] = \left(\frac{K_z}{L}\right) \begin{bmatrix} \ddots & & \vdots & & \iddots \\ & 1 & 1 & 1 & \\ \cdots & 1 & 1 & 1 & \cdots \\ & 1 & 1 & 1 & \\ \iddots & & \vdots & & \ddots \end{bmatrix}, \tag{83}$$

$$[\mathbf{R}] = \left(\frac{h\hat{K}_x}{2L}\right) \begin{bmatrix} \ddots & & \vdots & & \iddots \\ & k_{-1}k_{-1} & k_{-1}k_0 & k_{-1}k_1 & \\ \cdots & k_0 k_{-1} & k_0 k_0 & k_0 k_1 & \cdots \\ & k_1 k_{-1} & k_1 k_0 & k_1 k_1 & \\ \iddots & & \vdots & & \ddots \end{bmatrix} \tag{84}$$

and

$$\{\mathbf{f}\} = \left\{ \cdots \quad 0 \quad -2P_I \quad 0 \quad \cdots \right\}^{\mathrm{T}}. \tag{85}$$

In Eq. (82), the indexed entry is

$$T_n = D(k_n^4 + k_n^2 k_y^2 + k_y^4) - \rho t \omega^2 + (\rho_f \omega^2 / i\gamma_n), \tag{86}$$

with

$$D = \frac{Et^3}{12(1 - \upsilon^2)}, \tag{87}$$

where t is the thickness of the plate, E is Young's modulus, and υ is Poisson's ratio.

Fig. 2 is a plot of the magnitude of the transfer function of the plate normal displacement (w) divided by the amplitude of the applied incident pressure field (P_I) versus spatial position in the x-direction at a frequency of 50 Hz, an x-direction
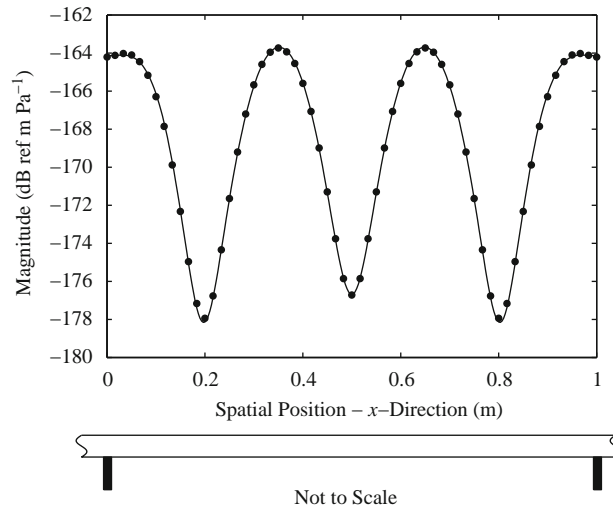

Fig. 2. Transfer function of z-direction displacement divided by incident pressure versus spatial location in the x-direction at 50 Hz for the thick plate system (____) and the thin plate system (●).
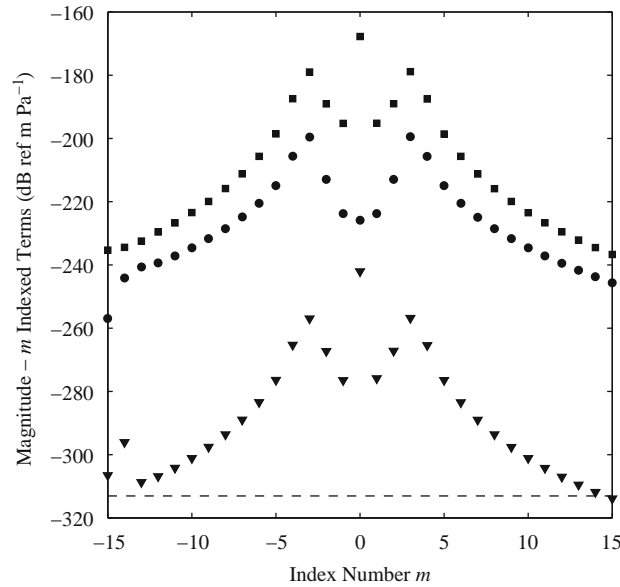
Fig. 3. Transfer function of $U_m^{(1)}(a)/P_I$ ($\bullet$), $V_m^{(1)}(a)/P_I$ ($\blacktriangledown$), and $W_m^{(1)}(a)/P_I$ ($\blacksquare$) versus index number. The dashed line is the machine precision of the computation.

wavenumber k_x of 0.0209 rad m^{-1} ($\theta=30^\circ$), and a y-direction wavenumber k_y of 0.0256 rad m^{-1} ($\phi=45^\circ$). The solid line is the elastic plate theory developed above and corresponds to Eq. (4) and the dot symbols are the Bernoulli–Euler plate theory and corresponds to Eq. (79). This example was generated using an extremely low frequency and small wavenumbers because this is a region in which the thick plate model should theoretically agree with the thin plate model. The following parameters were used for the plate: total plate thickness t is 0.01 m, plate densities ρ_1 and ρ_2 are 1200 kg m^{-3}, Lamé constants λ_1 and λ_2 are 9.31×10^8 N m^{-2}, Lamé constants μ_1 and μ_2 are 1.03×10^8 N m^{-2}, fluid density ρ_f is 1025 kg m^{-3}, fluid compressional wave speed c_f is 1500 m s^{-1} and spatial location y is 0. The following parameters were used for the ribs: width is 0.0064 m, height is 0.1016 m, Young's modulus is 200×10^9 N m^{-2}, Poisson's ratio is 0.3, density is 7860 kg m^{-3}, shear coefficient is 0.833 and rib separation distance L is 1.0 m. These parameters result in computed dynamic rib stiffnesses $\hat{K}_x$ equal to 7.955×10^3 N m^{-1}, K_y equal to 4.159×10^5 N m^{-2}, and K_z equal to 5.005×10^5 N m^{-2}. For the thick plate model, the plate interface region location b is -0.006 m and the output location is $z=-t/2$, which is -0.005 m. These parameters produced a dimensionless fluid wavenumber multiplied by plate height ($k_f h$) equal to 0.0021, which is a very small number where Bernoulli-Euler plate theory is considered accurate. The elastic plate model was truncated to 15 modes that produced a 120-by-120 system matrix and the thin plate model was truncated to 201 modes. There is almost total agreement between the two models over all of the abscissa values. To illustrate the convergence of the individual terms from the series solutions in Eqs. (2)–(4), each term is plotted versus the index number in Fig. 3. In this plot, the square markers are the terms $W_m^{(1)}(a)/P_I$, the circular markers are the terms $U_m^{(1)}(a)/P_I$, the triangular markers are the terms $V_m^{(1)}(a)/P_I$, and the dashed line is the working precision of the computation using 64-bit arithmetic numbers. For this validation problem, there is 46.2 dB of falloff for $U_m^{(1)}(a)/P_I$, a 57.1 dB of falloff for $V_m^{(1)}(a)/P_I$, and a 57.8 dB of falloff of $W_m^{(1)}(a)/P_I$ between the 3rd and 15th mode. For comparison, a $1/m^2$ convergent series has a 28.0 dB falloff between the 3rd and 15th term. Other tests of these series using various parameters resulted in similar behavior, however, as frequency increased, more terms were needed to insure the sum of the series has converged.

5. An example problem

An example problem is now formulated and discussed. This problem consists of a 0.0065-m (0.25-inch) thick aluminum plate coated with a 0.0254-m (1-inch) thick urethane polymer coating. This example was generated with the following plate parameters: aluminum Lamé constant λ_1 is 5.11×10^{10} N m^{-2}, Lamé constant μ_1 is 2.63×10^{10} N m^{-2}, density ρ_1 is 2710 kg m^{-3}, urethane Lamé constant λ_2 is 2.09×10^9 N m^{-2}, Lamé constant μ_2 is 7.14×10^7 N m^{-2}, density ρ_2 is 1110 kg m^{-3}, urethane structural loss factor is 0.05, fluid-compressional wave speed c_f is 1475 m s^{-1} and fluid density ρ_f is 1025 kg m^{-3}. The following parameters were used for the ribs: width is 0.0064 m, height is 0.1524 m, Young's modulus is 70×10^9 N m^{-2}, Poisson's ratio is 0.33, density is 2710 kg m^{-3}, shear coefficient is 0.833 and rib separation distance L is 1.0 m. No structural loss factors are used for the hull or ribs because they are typically metallic for a marine vehicle and have an extremely low loss factor, however, this term can be included in the analysis using complex material properties for these components. For this example, the material properties are considered constant over all frequencies

that the analysis is undertaken. Frequency dependent material properties can easily be incorporated into the model if needed. The problem is investigated from three technical standpoints: (1) the dynamic response of the structure, (2) the reception of an acoustic signal from within the structure, and (3) the scattered pressure field of an acoustic emission directed at the system.

Fig. 4 is a plot of the normal stress in the z-direction versus x-spatial position and frequency. This plot is at the midpoint of the combined plate system which is $z=-0.0159$ m (the top of the plate system is $z=0$), the value of y is 0, and the incoming acoustic wave has wavenumbers of $k_x=0$ and $k_y=0$. The scale of the plot is power in decibels and the units are dimensionless. In addition to the normal stress in the z-direction, the normal stresses in the x- and y-directions, the shear stresses in the xy-, xz- and yz-directions, and the displacements in the x-, y- and z-directions are available from the model. This provides a three-dimensional elastic analysis of this system. Note that if there were no ribs present in the system, this plot would be constant in the x-spatial position direction. The ribs introduce dynamic effects and this results in spatially varying stress and displacement fields. This amount of variation is dependent on the stiffness of the plate system with respect to the stiffness and spacing of the ribs.

The reception of an acoustic signal in the urethane can be accomplished by an internal array of sensors embedded in the coating. For the above example problem, an eight-element linear array of sensors that has an element-to-element spacing of 0.2 m and the first sensor located at $x=0.02$ m is analyzed. The array is oriented such that it is parallel to the x-axis. The length of this array makes it cross one rib in the structure, and the effect on the response of this crossing must be incorporated into the analysis. The magnitude of the response of two points at a distance L apart are identical; however, the phase angle must be adjusted to account for the orientation of the acoustic wave to the structure. This will result in a phase angle difference of two points a distance L apart of $k_x L$ radians. Fig. 5 is a plot of the normalized summed array response versus arrival angle at 3600 Hz, which is approximately the Nyquist frequency of the array. The summed array response was computed using

$$B(k_x,\omega) = \sum_{n=1}^{N} \Pi(x_n,0,z_s,\omega)\exp(-\mathrm{i}k_s x_n), \qquad (88)$$

where Π is the field variable of the sensor response, N is the number of sensors in the array, k_s is the steered wavenumber of the array with respect to the x-axis, and x_n is the location of the nth sensor. In Fig. 5, the solid line in the top plot corresponds to an array of z-direction displacement type sensors (typically an accelerometer) and the solid line in the bottom plot corresponds to an array of z-direction stress type sensors (typically a hydrophone). In both the top and the bottom plots, the dashed line corresponds to an array response in the system without ribs. In this example, the incoming acoustic wave has wavenumbers of $k_x=0$ and $k_y=0$. The plots are not symmetric about the steer angle of $0°$ because the array is not symmetric with respect to the structure. For this example, the interaction of the ribs with the sensor field is significant for the stress sensors, as the array response produces higher sidelobe levels than an ideal array would produce. There is a smaller effect of the ribs on the summed array response of displacement sensors, although there is still some increase in the sidelobe levels. Note that the array analysis can also be conducted using a planar array embedded in the coating, and the resulting beam pattern would be two-dimensional.
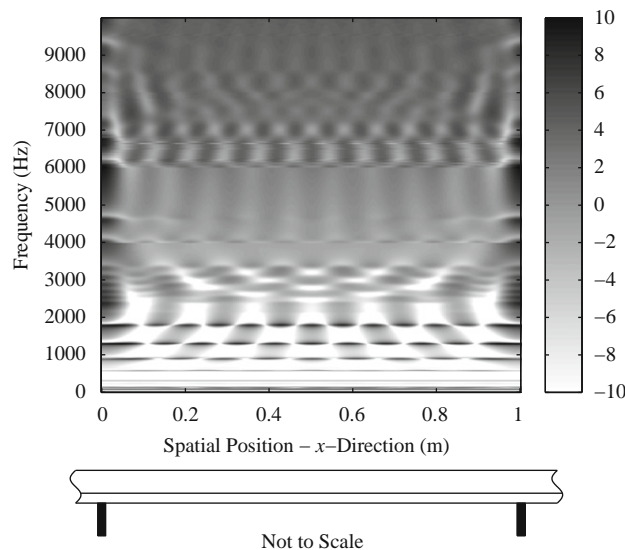

Fig. 4. Transfer function of z-direction normal stress divided by incident pressure versus spatial position in the x-direction and frequency for the thick plate system.
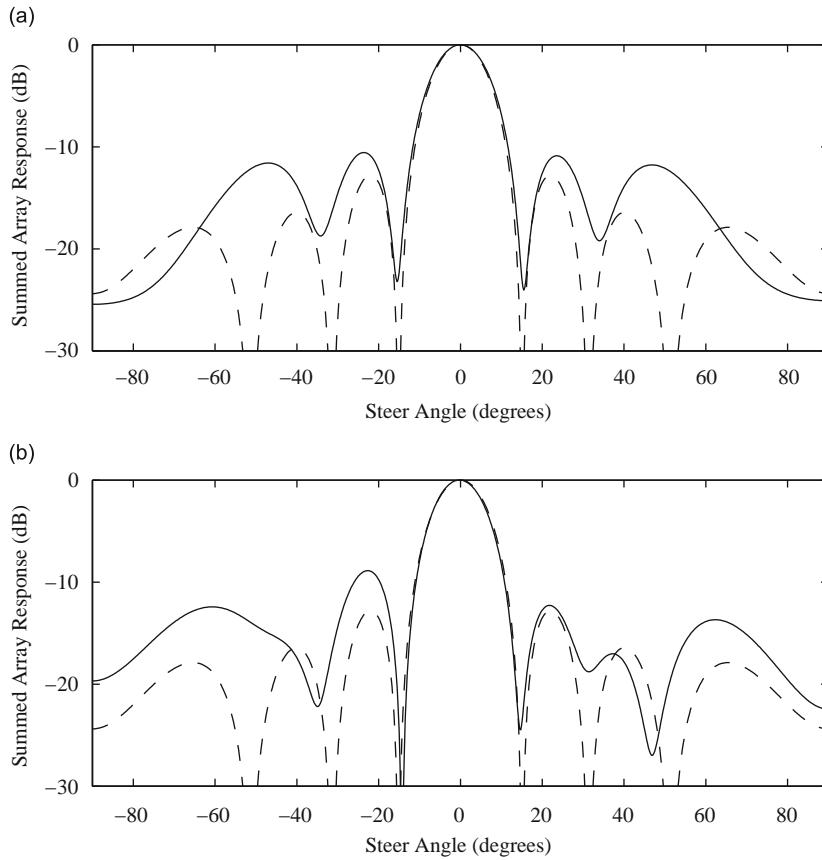
(a)

(b)

Fig. 5. Summed acoustic response versus steer angle for an array of (a) *z*-direction displacement sensors (———) and (b) *z*-direction normal stress sensors (———) compared to thick plate system without ribs (————).

In underwater structures, the scattered pressure field is an important quantity for quiet operation. The scattered pressure field divided by the incident pressure field is given by the expression

$$\frac{P_s(x,y,\omega)}{P_I} = \exp(ik_x x)\exp(ik_y y) + \sum_{m=-\infty}^{m=+\infty} \frac{\omega^2 \rho_f}{i\gamma_m} W_m^{(2)}(0)\exp(ik_m x)\exp(ik_y y), \tag{89}$$

where $P_s(x,y,\omega)$ is the scattered pressure field in the spatial-frequency domain, the first term on the right-hand side is the reflected pressure field, and the second term on the right-hand side is the radiated pressure field caused by normal displacement of the plate. Fig. 6 is a plot of the scattered pressure field divided by the incident pressure field versus *x*-spatial position and frequency. The incoming acoustic wave has wavenumbers of $k_x=0$ and $k_y=0$. The scale of the plot is power in decibels and the units are dimensionless. The scattered pressure field also has spatial variation in the *x*-direction.

The above simulations (and others) were run using all three nonzero dynamic stiffness values. These were compared to simulations where $\hat{K}_x = K_y = 0$ and this resulted in nearly identical values for the displacements, stresses and scattered pressure fields. This result makes sense physically because the dynamic stiffnesses $\hat{K}_x$ and K_y act on the in-plane displacement fields of the plates while K_z acts on the normal displacement field. Because the plate system is much stiffer in-plane, the contribution of stiffeners in these directions will be minimal. Utilizing the fact that the dominant beam stiffness effects are in the *z*-direction of the system, an upper frequency limit of the model can be determined. For the Timoshenko beam, the upper frequency is usually given by

$$\omega_{\text{MAX}} = \sqrt{\frac{\kappa A G}{\rho I}}. \tag{90}$$

For a rectangular beam, this expression can be approximated by

$$f_{\text{MAX}} \approx \frac{c_s}{2h}, \tag{91}$$

where f_{MAX} has units of Hz, c_s is the shear wave speed in the beam and h is the height of the beam. For the example problem presented here, this upper frequency limit is computed to be 10,290 Hz. The plate equations without the ribs have no upper frequency bound as these equations of motion are fully elastic.
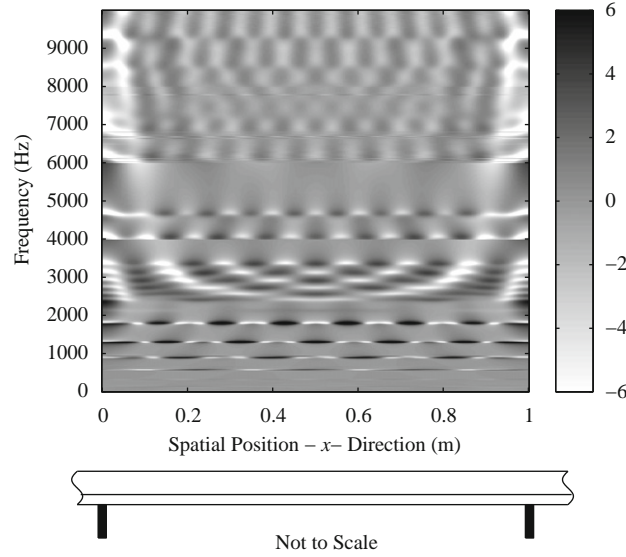
Fig. 6. Transfer function of scattered pressure field divided by incident pressure versus spatial position in the x-direction and frequency for the thick plate system.

6. Conclusions

An elastic analytical model of a system that consists of a ribbed plate covered by a fluid-loaded acoustical coating has been derived. This model was developed so that structural acoustic modeling of such a system could be undertaken at higher wavenumbers and frequencies, rather than the previously available low frequency and low wavenumber models. The new model has been shown to agree with previously developed thin plate solutions to the problem at low frequency. An example problem was developed to illustrate high-frequency behavior and an analysis of the dynamic response, acoustic reception, and scattered acoustic field is included. It was shown that for this example, the ribs have a significant effect on the high frequency dynamic response of the structure.

Acknowledgements

Appendix A. Double summation identities

A proof of the double summation identities used in Eq. (58) is developed here. Starting with the series G_m (where G_m equals either $W_m^{(1)}(a)$, $V_m^{(1)}(a)$, or $ik_m W_m^{(1)}(a)$), the following expression is written as:

$$\sum_{n=-\infty}^{n=+\infty} [\sum_{m=-\infty}^{m=+\infty} G_m \exp(ik_m x)] \exp\left(\frac{i2\pi nx}{L}\right). \tag{A.1}$$

Using the definition of k_m from Eq. (5) yields

$$\exp(ik_x x) \sum_{n=-\infty}^{n=+\infty} \left[\sum_{m=-\infty}^{m=+\infty} G_m \exp\left(\frac{i2\pi mx}{L}\right)\right] \exp\left(\frac{i2\pi nx}{L}\right). \tag{A.2}$$

Expanding the m indexed series results in

$$\exp(ik_x x) \sum_{n=-\infty}^{n=+\infty} \left[\cdots + G_{-1} \exp\left(\frac{i2\pi(-1)x}{L}\right) + G_0 \exp\left(\frac{i2\pi 0x}{L}\right) + G_1 \exp\left(\frac{i2\pi 1x}{L}\right) + \cdots\right] \exp\left(\frac{i2\pi nx}{L}\right). \tag{A.3}$$

Next, expanding the n indexed series yields

$$\exp(ik_x x) \left\{\cdots + \left[\cdots + G_{-1} \exp\left(\frac{i2\pi(-1)x}{L}\right) + G_0 \exp\left(\frac{i2\pi 0x}{L}\right) + G_1 \exp\left(\frac{i2\pi 1x}{L}\right) + \cdots\right] \exp\left(\frac{i2\pi(-1)x}{L}\right)\right.$$

$$+\left[\cdots+G_{-1}\exp\left(\frac{\mathrm{i}2\pi(-1)x}{L}\right)+G_0\exp\left(\frac{\mathrm{i}2\pi0x}{L}\right)+G_1\exp\left(\frac{\mathrm{i}2\pi1x}{L}\right)+\cdots\right]\exp\left(\frac{\mathrm{i}2\pi0x}{L}\right)$$
$$+\left[\cdots+G_{-1}\exp\left(\frac{\mathrm{i}2\pi(-1)x}{L}\right)+G_0\exp\left(\frac{\mathrm{i}2\pi0x}{L}\right)+G_1\exp\left(\frac{\mathrm{i}2\pi1x}{L}\right)+\cdots\right]\exp\left(\frac{\mathrm{i}2\pi1x}{L}\right)+\cdots\Big\}. \tag{A.4}$$

Incorporating the outer exponentials into the inner exponentials gives

$$\exp(\mathrm{i}k_xx)\Big\{\cdots+\left[\cdots+G_{-1}\exp\left(\frac{\mathrm{i}2\pi(-2)x}{L}\right)+G_0\exp\left(\frac{\mathrm{i}2\pi(-1)x}{L}\right)+G_1\exp\left(\frac{\mathrm{i}2\pi0x}{L}\right)+\cdots\right]$$
$$+\left[\cdots+G_{-1}\exp\left(\frac{\mathrm{i}2\pi(-1)x}{L}\right)+G_0\exp\left(\frac{\mathrm{i}2\pi0x}{L}\right)+G_1\exp\left(\frac{\mathrm{i}2\pi1x}{L}\right)+\cdots\right]$$
$$+\left[\cdots+G_{-1}\exp\left(\frac{\mathrm{i}2\pi0x}{L}\right)+G_0\exp\left(\frac{\mathrm{i}2\pi1x}{L}\right)+G_1\exp\left(\frac{\mathrm{i}2\pi2x}{L}\right)+\cdots\right]+\cdots\Big\}. \tag{A.5}$$

Summing the above expression diagonally using similar exponentials results in

$$\exp(\mathrm{i}k_xx)\left[\cdots+\sum_{n=-\infty}^{n=+\infty}G_n\exp\left(\frac{\mathrm{i}2\pi(-1)x}{L}\right)+\sum_{n=-\infty}^{n=+\infty}G_n\exp\left(\frac{\mathrm{i}2\pi(0)x}{L}\right)+\sum_{n=-\infty}^{n=+\infty}G_n\exp\left(\frac{\mathrm{i}2\pi(1)x}{L}\right)+\cdots\right]. \tag{A.6}$$

Factoring out the G_n series yields the expression

$$\exp(\mathrm{i}k_xx)\sum_{n=-\infty}^{n=+\infty}G_n\left[\cdots+\exp\left(\frac{\mathrm{i}2\pi(-1)x}{L}\right)+\exp\left(\frac{\mathrm{i}2\pi(0)x}{L}\right)+\exp\left(\frac{\mathrm{i}2\pi(1)x}{L}\right)+\cdots\right] \tag{A.7}$$

which can be rewritten as

$$\exp(\mathrm{i}k_xx)[\sum_{n=-\infty}^{n=+\infty}G_n]\sum_{m=-\infty}^{m=+\infty}\exp\left(\frac{\mathrm{i}2\pi mx}{L}\right). \tag{A.8}$$

Finally, incorporating the leading exponential into the m indexed series gives the expression

$$[\sum_{n=-\infty}^{n=+\infty}G_n]\sum_{m=-\infty}^{m=+\infty}\exp(\mathrm{i}k_mx). \tag{A.9}$$

Appendix B. Matrix and vector entries

The entries of the matrixes and vectors in Eq. (71) are listed below. Without loss of generality, the top of the top plate is defined as $z=c=0$. For the $[\mathbf{A}k_n]$ matrix, the nonzero entries are

$$a_{1,1}=\{-\lambda_1[(\alpha_n^{(1)})^2+k_n^2+k_y^2)]-2\mu_1(\alpha_n^{(1)})^2\}\cos(\alpha_n^{(1)}a),$$

$$a_{1,2}=\{-\lambda_1[(\alpha_n^{(1)})^2+k_n^2+k_y^2)]-2\mu_1(\alpha_n^{(1)})^2\}\sin(\alpha_n^{(1)}a),$$

$$a_{1,3}=2\mathrm{i}\mu_1\beta_n^{(1)}k_y\sin(\beta_n^{(1)}a),$$

$$a_{1,4}=-2\mathrm{i}\mu_1\beta_n^{(1)}k_y\cos(\beta_n^{(1)}a),$$

$$a_{1,5}=-2\mathrm{i}\mu_1\beta_n^{(1)}k_n\sin(\beta_n^{(1)}a),$$

$$a_{1,6}=2\mathrm{i}\mu_1\beta_n^{(1)}k_n\cos(\beta_n^{(1)}a),$$

$$a_{2,1}=-2\mathrm{i}\mu_1\alpha_n^{(1)}k_y\sin(\alpha_n^{(1)}a),$$

$$a_{2,2}=2\mathrm{i}\mu_1\alpha_n^{(1)}k_y\cos(\alpha_n^{(1)}a),$$

$$a_{2,3}=-\mu_1[(\beta_n^{(1)})^2+k_n^2-k_y^2]\cos(\beta_n^{(1)}a),$$

$$a_{2,4}=-\mu_1[(\beta_n^{(1)})^2+k_n^2-k_y^2]\sin(\beta_n^{(1)}a),$$

$$a_{2,5}=-2\mu_1k_yk_n\cos(\beta_n^{(1)}a),$$

$$a_{2,6}=-2\mu_1k_yk_n\sin(\beta_n^{(1)}a),$$

$$a_{3,1}=-2\mathrm{i}\mu_1\alpha_n^{(1)}k_n\sin(\alpha_n^{(1)}a),$$

$$a_{3,2} = 2\mathrm{i}\mu_1\alpha_n^{(1)}k_n\cos(\alpha_n^{(1)}a),$$

$$a_{3,3} = 2\mu_1 k_n k_y\cos(\beta_n^{(1)}a),$$

$$a_{3,4} = 2\mu_1 k_n k_y\sin(\beta_n^{(1)}a),$$

$$a_{3,5} = \mu_1[(\beta_n^{(1)})^2-k_n^2+k_y^2]\cos(\beta_n^{(1)}a),$$

$$a_{3,6} = \mu_1[(\beta_n^{(1)})^2-k_n^2+k_y^2]\sin(\beta_n^{(1)}a),$$

$$a_{4,1} = \{-\lambda_1[(\alpha_n^{(1)})^2+k_n^2+k_y^2]-2\mu_1(\alpha_n^{(1)})^2\}\cos(\alpha_n^{(1)}b),$$

$$a_{4,2} = \{-\lambda_1[(\alpha_n^{(1)})^2+k_n^2+k_y^2]-2\mu_1(\alpha_n^{(1)})^2\}\sin(\alpha_n^{(1)}b),$$

$$a_{4,3} = 2\mathrm{i}\mu_1\beta_n^{(1)}k_y\sin(\beta_n^{(1)}b),$$

$$a_{4,4} = -2\mathrm{i}\mu_1\beta_n^{(1)}k_y\cos(\beta_n^{(1)}b),$$

$$a_{4,5} = -2\mathrm{i}\mu_1\beta_n^{(1)}k_n\sin(\beta_n^{(1)}b),$$

$$a_{4,6} = 2\mathrm{i}\mu_1\beta_n^{(1)}k_n\cos(\beta_n^{(1)}b),$$

$$a_{4,7} = \{\lambda_2[(\alpha_n^{(2)})^2+k_n^2+k_y^2]+2\mu_2(\alpha_n^{(2)})^2\}\cos(\alpha_n^{(2)}b),$$

$$a_{4,8} = \{\lambda_2[(\alpha_n^{(2)})^2+k_n^2+k_y^2]+2\mu_2(\alpha_n^{(2)})^2\}\sin(\alpha_n^{(2)}b),$$

$$a_{4,9} = -2\mathrm{i}\mu_2\beta_n^{(2)}k_y\sin(\beta_n^{(2)}b),$$

$$a_{4,10} = 2\mathrm{i}\mu_2\beta_n^{(2)}k_y\cos(\beta_n^{(2)}b),$$

$$a_{4,11} = 2\mathrm{i}\mu_2\beta_n^{(2)}k_n\sin(\beta_n^{(2)}b),$$

$$a_{4,12} = -2\mathrm{i}\mu_2\beta_n^{(2)}k_n\cos(\beta_n^{(2)}b),$$

$$a_{5,1} = -2\mathrm{i}\mu_1\alpha_n^{(1)}k_y\sin(\alpha_n^{(1)}b),$$

$$a_{5,2} = 2\mathrm{i}\mu_1\alpha_n^{(1)}k_y\cos(\alpha_n^{(1)}b),$$

$$a_{5,3} = -\mu_1[(\beta_n^{(1)})^2+k_n^2-k_y^2]\cos(\beta_n^{(1)}b),$$

$$a_{5,4} = -\mu_1[(\beta_n^{(1)})^2+k_n^2-k_y^2]\sin(\beta_n^{(1)}b),$$

$$a_{5,5} = -2\mu_1 k_y k_n\cos(\beta_n^{(1)}b),$$

$$a_{5,6} = -2\mu_1 k_y k_n\sin(\beta_n^{(1)}b),$$

$$a_{5,7} = 2\mathrm{i}\mu_2\alpha_n^{(2)}k_y\sin(\alpha_n^{(2)}b),$$

$$a_{5,8} = -2\mathrm{i}\mu_2\alpha_n^{(2)}k_y\cos(\alpha_n^{(2)}b),$$

$$a_{5,9} = \mu_2[(\beta_n^{(2)})^2+k_n^2-k_y^2]\cos(\beta_n^{(2)}b),$$

$$a_{5,10} = \mu_2[(\beta_n^{(2)})^2+k_n^2-k_y^2]\sin(\beta_n^{(2)}b),$$

$$a_{5,11} = 2\mu_2 k_y k_n\cos(\beta_n^{(2)}b),$$

$$a_{5,12} = 2\mu_2 k_y k_n\sin(\beta_n^{(2)}b),$$

$$a_{6,1} = -2\mathrm{i}\mu_1\alpha_n^{(1)}k_n\sin(\alpha_n^{(1)}b),$$

$$a_{6,2} = 2i\mu_1\alpha_n^{(1)}k_n\cos(\alpha_n^{(1)}b),$$

$$a_{6,3} = 2\mu_1 k_n k_y \cos(\beta_n^{(1)}b),$$

$$a_{6,4} = 2\mu_1 k_n k_y \sin(\beta_n^{(1)}b),$$

$$a_{6,5} = \mu_1[(\beta_n^{(1)})^2 - k_n^2 + k_y^2]\cos(\beta_n^{(1)}b),$$

$$a_{6,6} = \mu_1[(\beta_n^{(1)})^2 - k_n^2 + k_y^2]\sin(\beta_n^{(1)}b),$$

$$a_{6,7} = 2i\mu_2\alpha_n^{(2)}k_n\sin(\alpha_n^{(2)}b),$$

$$a_{6,8} = -2i\mu_2\alpha_n^{(2)}k_n\cos(\alpha_n^{(2)}b),$$

$$a_{6,9} = -2\mu_2 k_n k_y \cos(\beta_n^{(2)}b),$$

$$a_{6,10} = -2\mu_2 k_n k_y \sin(\beta_n^{(2)}b),$$

$$a_{6,11} = -\mu_2[(\beta_n^{(2)})^2 - k_n^2 + k_y^2]\cos(\beta_n^{(2)}b),$$

$$a_{6,12} = -\mu_2[(\beta_n^{(2)})^2 - k_n^2 + k_y^2]\sin(\beta_n^{(2)}b),$$

$$a_{7,1} = ik_n\cos(\alpha_n^{(1)}b),$$

$$a_{7,2} = ik_n\sin(\alpha_n^{(1)}b),$$

$$a_{7,3} = \frac{k_n k_y}{\beta_n^{(1)}}\sin(\beta_n^{(1)}b),$$

$$a_{7,4} = \frac{-k_n k_y}{\beta_n^{(1)}}\cos(\beta_n^{(1)}b),$$

$$a_{7,5} = \left(\beta_n^{(1)} + \frac{k_y^2}{\beta_n^{(1)}}\right)\sin(\beta_n^{(1)}b),$$

$$a_{7,6} = -\left(\beta_n^{(1)} + \frac{k_y^2}{\beta_n^{(1)}}\right)\cos(\beta_n^{(1)}b),$$

$$a_{7,7} = -ik_n\cos(\alpha_n^{(2)}b),$$

$$a_{7,8} = -ik_n\sin(\alpha_n^{(2)}b),$$

$$a_{7,9} = \frac{-k_n k_y}{\beta_n^{(2)}}\sin(\beta_n^{(2)}b),$$

$$a_{7,10} = \frac{k_n k_y}{\beta_n^{(2)}}\cos(\beta_n^{(2)}b),$$

$$a_{7,11} = -\left(\beta_n^{(2)} + \frac{k_y^2}{\beta_n^{(2)}}\right)\sin(\beta_n^{(2)}b),$$

$$a_{7,12} = \left(\beta_n^{(2)} + \frac{k_y^2}{\beta_n^{(2)}}\right)\cos(\beta_n^{(2)}b),$$

$$a_{8,1} = ik_y\cos(\alpha_n^{(1)}b),$$

$$a_{8,2} = ik_y\sin(\alpha_n^{(1)}b),$$

$$a_{8,3} = -\left(\beta_n^{(1)} + \frac{k_n^2}{\beta_n^{(1)}}\right)\sin(\beta_n^{(1)}b),$$

$$a_{8,4} = \left(\beta_n^{(1)} + \frac{k_n^2}{\beta_n^{(1)}}\right)\cos(\beta_n^{(1)}b),$$

$$a_{8,5} = \frac{-k_n k_y}{\beta_n^{(1)}}\sin(\beta_n^{(1)}b),$$

$$a_{8,6} = \frac{k_n k_y}{\beta_n^{(1)}}\cos(\beta_n^{(1)}b),$$

$$a_{8,7} = -\mathrm{i}k_y\cos(\alpha_n^{(2)}b),$$

$$a_{8,8} = -\mathrm{i}k_y\sin(\alpha_n^{(2)}b),$$

$$a_{8,9} = \left(\beta_n^{(2)} + \frac{k_n^2}{\beta_n^{(2)}}\right)\sin(\beta_n^{(2)}b),$$

$$a_{8,10} = -\left(\beta_n^{(2)} + \frac{k_n^2}{\beta_n^{(2)}}\right)\cos(\beta_n^{(2)}b),$$

$$a_{8,11} = \frac{k_n k_y}{\beta_n^{(2)}}\sin(\beta_n^{(2)}b),$$

$$a_{8,12} = \frac{-k_n k_y}{\beta_n^{(2)}}\cos(\beta_n^{(2)}b),$$

$$a_{9,1} = -\alpha_n^{(1)}\sin(\alpha_n^{(1)}b),$$

$$a_{9,2} = \alpha_n^{(1)}\cos(\alpha_n^{(1)}b),$$

$$a_{9,3} = -\mathrm{i}k_y\cos(\beta_n^{(1)}b),$$

$$a_{9,4} = -\mathrm{i}k_y\sin(\beta_n^{(1)}b),$$

$$a_{9,5} = \mathrm{i}k_n\cos(\beta_n^{(1)}b),$$

$$a_{9,6} = \mathrm{i}k_n\sin(\beta_n^{(1)}b),$$

$$a_{9,7} = \alpha_n^{(2)}\sin(\alpha_n^{(2)}b),$$

$$a_{9,8} = -\alpha_n^{(2)}\cos(\alpha_n^{(2)}b),$$

$$a_{9,9} = \mathrm{i}k_y\cos(\beta_n^{(2)}b),$$

$$a_{9,10} = \mathrm{i}k_y\sin(\beta_n^{(2)}b),$$

$$a_{9,11} = -\mathrm{i}k_n\cos(\beta_n^{(2)}b),$$

$$a_{9,12} = -\mathrm{i}k_n\sin(\beta_n^{(2)}b),$$

$$a_{10,7} = -\lambda_2[(\alpha_n^{(2)})^2 + k_n^2 + k_y^2] - 2\mu_2(\alpha_n^{(2)})^2,$$

$$a_{10,8} = \frac{\omega^2\rho_f\alpha_n^{(2)}}{\mathrm{i}\gamma_n},$$

$$a_{10,9} = \frac{-\omega^2\rho_f k_y}{\gamma_n},$$

$$a_{10,10} = -2\mathrm{i}\mu_2\beta_n^{(2)}k_y,$$

$$a_{10,11} = \frac{\omega^2\rho_f k_n}{\gamma_n},$$

$$a_{10,12} = 2\mathrm{i}\mu_2\beta_n^{(2)}k_n,$$

$$a_{11,8} = 2\mathrm{i}\mu_2\alpha_n^{(2)}k_y,$$

$$a_{11,9} = -\mu_2(\beta_n^{(2)} + k_n^2 - k_y^2),$$

$$a_{11,11} = -2\mu_2 k_n k_y,$$

$$a_{12,8} = 2\mathrm{i}\mu_2\alpha_n^{(2)}k_n,$$

$$a_{12,9} = 2\mu_2 k_n k_y,$$

and

$$a_{12,11} = \mu_2[(\beta_n^{(2)})^2 - k_n^2 + k_y^2].$$

The nonzero entries of the $[\mathbf{F}(k_n)]$ matrix are

$$f_{1,1} = -(K_z/L)\alpha_n^{(1)}\sin(\alpha_n^{(1)}a),$$

$$f_{1,2} = (K_z/L)\alpha_n^{(1)}\cos(\alpha_n^{(1)}a),$$

$$f_{1,3} = -(K_z/L)\mathrm{i}k_y\cos(\beta_n^{(1)}a),$$

$$f_{1,4} = -(K_z/L)\mathrm{i}k_y\sin(\beta_n^{(1)}a),$$

$$f_{1,5} = (K_z/L)\mathrm{i}k_n\cos(\beta_n^{(1)}a),$$

$$f_{1,6} = (K_z/L)\mathrm{i}k_n\sin(\beta_n^{(1)}a).$$

$$f_{2,1} = (K_y/L)\mathrm{i}k_y\cos(\alpha_n^{(1)}a),$$

$$f_{2,2} = (K_y/L)\mathrm{i}k_y\sin(\alpha_n^{(1)}a),$$

$$f_{2,3} = -(K_y/L)\left(\beta_n^{(1)} + \frac{k_n^2}{\beta_n^{(1)}}\right)\sin(\beta_n^{(1)}a),$$

$$f_{2,4} = (K_y/L)\left(\beta_n^{(1)} + \frac{k_n^2}{\beta_n^{(1)}}\right)\cos(\beta_n^{(1)}a),$$

$$f_{2,5} = -(K_y/L)\frac{k_n k_y}{\beta_n^{(1)}}\sin(\beta_n^{(1)}a),$$

$$f_{2,6} = (K_y/L)\frac{k_n k_y}{\beta_n^{(1)}}\cos(\beta_n^{(1)}a),$$

$$f_{3,1} = -(\mathrm{i}k_n\hat{K}_x/L)\alpha_n^{(1)}\sin(\alpha_n^{(1)}a),$$

$$f_{3,2} = (\mathrm{i}k_n\hat{K}_x/L)\alpha_n^{(1)}\cos(\alpha_n^{(1)}a),$$

$$f_{3,3} = -(\mathrm{i}k_n\hat{K}_x/L)\mathrm{i}k_y\cos(\beta_n^{(1)}a),$$

$$f_{3,4} = -(\mathrm{i}k_n\hat{K}_x/L)\mathrm{i}k_y\sin(\beta_n^{(1)}a),$$

$$f_{3,5} = (\mathrm{i}k_n\hat{K}_x/L)\mathrm{i}k_n\cos(\beta_n^{(1)}a),$$

and

$$f_{3,6} = (\mathrm{i}k_n\hat{K}_x/L)\mathrm{i}k_n\sin(\beta_n^{(1)}a).$$

The entries of the **p** vector are

$$\mathbf{p} = [0 \quad 0 \quad 0 \quad 0 \quad 0 \quad 0 \quad 0 \quad 0 \quad 0 \quad -2P_I \quad 0 \quad 0]^{\mathrm{T}}.$$

References

[1] S.M. Han, H. Benaroya, T. Wei, Dynamics of transversely vibrating beams using four engineering theories, *Journal of Sound and Vibration* 225 (5) (1999) 935–988.

[2] R.D. Mindlin, Influence of rotary inertia and shear on flexural motions of isotropic plates, *Journal of Applied Mechanics* 18 (1951) 31–38.

[3] L.M. Brekhovskikh, *Waves in Layered Media*, Academic Press, San Diego, CA, 1980.

[4] D.G. Crighton, The free and forced waves on a fluid-loaded elastic plate, *Journal of Sound and Vibration* 63 (2) (1979) 225–235.

[5] D.L. Folds, C.D. Loggins, Transmission and reflection of ultrasonic waves in layered media, *Journal of the Acoustical Society of America* 62 (5) (1977) 1102–1109.

[6] D.J. Mead, K.K. Pujara, Space-harmonic analysis of a periodically supported beam: response to convected random loading, *Journal of Sound and Vibration* 14 (4) (1971) 525–541.

[7] B.R. Mace, Periodically stiffened fluid-loaded plates, I: response to convected harmonic pressure and free wave propagation, *Journal of Sound and Vibration* 73 (4) (1980) 473–486.

[8] B.R. Mace, Periodically stiffened fluid-loaded plates, II: response to line and point forces, *Journal of Sound and Vibration* 73 (4) (1980) 487–504.

[9] B.A. Cray, Acoustic radiation from periodic and sectionally aperiodic rib-stiffened plates, *Journal of the Acoustical Society of America* 95 (1) (1994) 256–264.

[10] G.P. Eatwell, D. Butler, The response of fluid-loaded, beam-stiffened plates, *Journal of Sound and Vibration* 84 (3) (1982) 371–388.

[11] G.P. Eatwell, Free-wave propagation in an irregularly stiffened, fluid loaded plate, *Journal of Sound and Vibration* 88 (4) (1983) 507–522.

[12] C.J. Chapman, S.V. Sorokin, The forced vibration of an elastic plate under significant fluid loading, *Journal of Sound and Vibration* 281 (3–5) (2005) 719–741.

[13] B.L. Woolley, Acoustic scattering from a submerged plate, II: finite number of reinforcing ribs, *Journal of the Acoustical Society of America* 67 (5) (1980) 1654–1658.

[14] B.P. Belinskii, Radiation of sound from a plate reinforced by a set of projecting beams under the action of a driving force, *Soviet Physics-Acoustics* 29 (4) (1983) 251–255.

[15] B.R. Mace, Sound radiation from fluid loaded orthogonally stiffened plates, *Journal of Sound and Vibration* 79 (3) (1981) 439–452.

[16] B.P. Belinskii, Diffraction of a plane wave by an infinite elastic plate stiffened by a doubly periodic set of rigid ribs, *Journal of Applied Mathematics and Mechanics* 47 (6) (1983) 767–774 (English reprint of *Prikladnaya Matematika I Mekhanika*).

[17] S.H. Ko, W. Seong, S. Pyo, Structure borne noise reduction for an infinite, elastic cylindrical shell, *Journal of the Acoustical Society of America* 109 (4) (2001) 1483–1495.

[18] J.M. Cuschieri, D. Feit, Influence of circumferential partial coating on the acoustic radiation from a fluid-loaded shell, *Journal of the Acoustical Society of America* 107 (6) (2000) 3196–3207.

[19] W. Zhang, A. Wang, N. Vlahopoulos, K. Wu, High-frequency vibration analysis of thin elastic plates under heavy fluid loading by an energy finite element formulation, *Journal of Sound and Vibration* 263 (1) (2003) 21–46.

[20] A.J. Hull, Dynamic response of an elastic plate containing periodic masses, *Journal of Sound and Vibration* 310 (1–2) (2008) 1–20.

[21] K.F. Graff, *Wave Motion in Elastic Solids*, Dover Publications, New York, 1975.